On the compressibility of TiC in microcrystalline and nanoparticulate form

2008 J. Phys.: Condens. Matter 20 445226

(http://iopscience.iop.org/0953-8984/20/44/445226)

J. Phys.: Condens. Matter **20** (2008) 445226 (6pp) doi:10.1088/0953-8984/20/44/445226

On the compressibility of TiC in microcrystalline and nanoparticulate form

Q F Gu[1], G Krauss[1], F Gramm[2] and W Steurer[1]

[1] Laboratory of Crystallography, Department of Materials, ETH Zurich, CH-8093 Zurich, Switzerland
[2] Electron Microscopy Center Zurich (EMEZ), ETH Zurich, CH-8093 Zurich, Switzerland

E-mail: guenter.krauss@mat.ethz.ch

Received 3 April 2008, in final form 1 July 2008
Published 10 October 2008
Online at stacks.iop.org/JPhysCM/20/445226

Abstract

The compressibility of TiC in microcrystalline and nanoparticulate (30–50 nm) form was studied by *in situ* high-pressure synchrotron radiation x-ray diffraction measurements up to 53.7 GPa using a diamond anvil cell. Both materials are structurally stable within the framework of the experiments applying quasihydrostatic pressure conditions. Under nonhydrostatic pressure conditions, the lattice of microcrystalline TiC is rhombohedrally distorted. Comparable values for the bulk modulus were found for both materials, i.e. $K_0 = 254(7)$ GPa, $K' = 4.8(4)$ for microcrystalline TiC and $K_0 = 276(14)$ GPa, $K' = 3.5(8)$ for nanoparticulate TiC, respectively. High-resolution transmission electron microscopy investigations revealed a nearly single-domain microstructure of the nanoparticles. The microstructure and size of the nanoparticles, making a size-induced effect on the mechanical properties negligible, explain well the observed similarity of the mechanical properties of microcrystalline and nanoparticulate TiC.

1. Introduction

For the change of a material's mechanical properties as a function of its particle size, when decreasing their size to the nanoscale (1–100 nm), controversial findings have been reported in the literature. The elastic modulus was found to be independent of the particle size as observed for Ni [1] nanoparticles in the range down to 20 nm. The bulk modulus increases with decreasing particle size, as was observed for example in γ-Fe_2O_3 [2], Au and Ag [3]. On the other hand, a decrease of the bulk modulus with decreasing particle size was observed, e.g. in ZnS [4] and CdSe [5]. To clarify these controversial findings, additional studies using defined and well-characterized nanoparticles are necessary to identify the influence not only from particle size, but also from the microstructure, synthesis conditions and morphology of the nanoparticles [6, 7]. These, often ignored, characteristics of the nanoparticles may have an important influence on their mechanical properties [3, 8].

Titanium carbide (TiC) was chosen for the present study, as it is a commonly used hard material with a variety of applications. It is characterized by a high melting temperature, high hardness as well as good electrical and thermal conductivity. TiC crystallizes with the NaCl structure type. The behaviour of microcrystalline (bulk) TiC (b-TiC) at high pressures has been studied experimentally and theoretically, and the presence of a rhombohedral high-pressure modification at $P > 18$ GPa was reported [9]. TiC nanoparticles (n-TiC) were used in advanced materials, such as e.g. nanocomposites or as nanocrystalline TiC in thin layers. Despite b-TiC not being naturally occurring, n-TiC has been found in cosmic dust [10]. The compressibility of TiC nanoparticles has not been studied yet. The common use of b-TiC and n-TiC, their interesting properties and the reported phase transition of b-TiC were the motivation of the present work.

2. Experimental details

The investigated materials were polycrystalline b-TiC (2N5 particle size 2–3 μm, Alfa Aesar) and n-TiC (2N, particle size 30–50 nm, Nanostructured & Amorphous Materials, Inc., USA). The carbon content was analyzed using a Leco RC-412 Multiphase Carbon Determinator. The obtained values x for carbon in TiC_x were $x > 0.99$ for b-TiC and $x > 0.98$ for n-TiC, respectively. Therefore both materials can be

regarded as stoichiometric TiC. The microstructural analysis of the nanoparticles was done using a Philips CM30 high-resolution transmission electron microscope (HRTEM). The lattice parameters were determined on a STOE stadi-P powder diffractometer using Co Kα_1 radiation and silicon (NBS640a) as internal standard. Synchrotron x-ray diffraction experiments were performed at the Materials Science beam line, Swiss Light Source (SLS) at the Paul Scherrer Institut (PSI, Villigen, Switzerland). 2D diffraction data was collected on a Marresearch mar345 image-plate detector using a wavelength of 0.5640 Å. The 2D data was integrated by the use of the program fit2d [11] and the 1D powder pattern were refined by applying the Rietveld-method using the program GSAS [12, 13] for lattice parameter determination. High pressures up to 48.3(2) GPa for b-TiC and 53.7(3) GPa for n-TiC were generated by use of an ETH-type diamond anvil cell [14]. Diamond anvils with culet diameter of 0.3 mm were used. The diameter of the hole in the preindented (0.06 mm) tungsten or rhenium gaskets was 0.125 mm. For quasihydrostatic conditions, a mixture of methanol and ethanol (4:1) served as the pressure-transmitting medium. To minimize deviatoric stress, the amount of sample covered only ca 70 % of the total volume (pressure medium ca 30%) within the gasket. Nonhydrostatic conditions were generated by filling the whole pressure chamber densely with the sample material without using a pressure medium. In both cases a ruby chip was placed into the sample chamber as a pressure marker and the pressures were determined using the ruby fluorescence technique. The equations of state were calculated by the use of the program EosFit5.2 [15]. Alternatively, the half-width at full maximum of the reflections was determined by fitting a pseudo-Voigt profile to the single reflections by using the program cmpr [16].

3. Results and discussion

The lattice parameters of the starting materials were determined as 4.326(3) Å and 4.321(5) Å for b-TiC and n-TiC, respectively, which are in good agreement with literature data for stoichiometric b-TiC (4.328(2) Å, [17]) and do not indicate a high amount of surface-induced strain on the nanoparticles.

3.1. High-pressure studies

High-pressure experiments were done in three different runs: (i) powder patterns were collected in small pressure steps up to ca 40 GPa. This data was used to calculate the compressibilities. (ii) Single measurements at the highest pressures reached with the used setup were done, i.e. at 53.7 GPa for n-Tic and 48.3 GPa for b-TiC, respectively, to identify a possible phase transition at the upper limit of the experiments. The data was not used for the calculation of the bulk modulus due to the inevitable offsets of the obtained lattice parameters from different runs using different loadings. (iii) b-TiC was measured without pressure medium up to ca 40 GPa, i.e. pressures well above the phase transition of 18 GPa reported in [9]. This data was used to identify the influence of the nonhydrostatic pressure conditions.

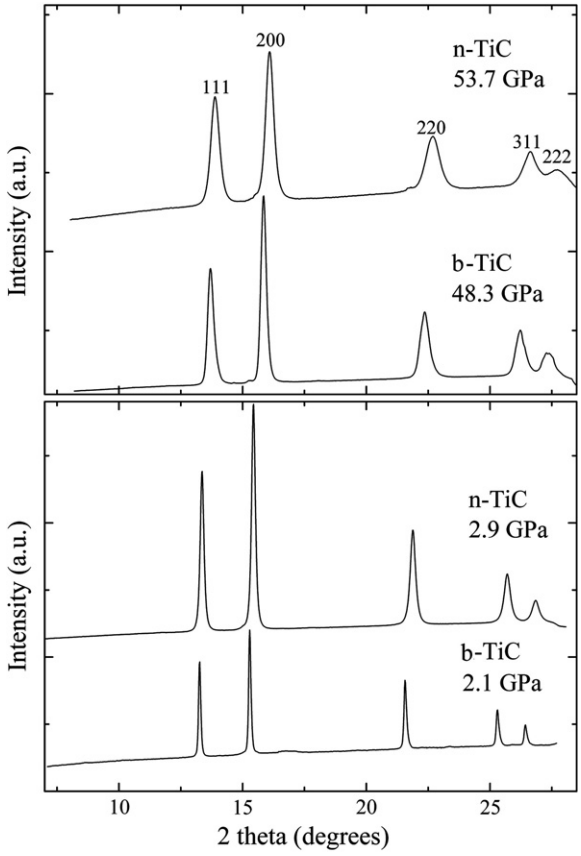

Figure 1. X-ray diffraction pattern of n-TiC and b-TiC at the lowest and highest pressures used in the experiment ($\lambda = 0.5640$ Å). The compounds are structurally stable within the framework of the experiment.

Quasihydrostatic conditions. TiC was found to be structurally stable in microcrystalline, as well as nanoparticulate form up to the highest pressures used in the experiments, i.e. 53.7 GPa for b-TiC and 48.7 GPa for n-TiC, respectively (figure 1). The observable peak broadening can be explained by the increasing strain caused by the increasing nonhydrostaticity of the pressure medium with increasing pressure. It has to be mentioned that all pressure media solidify at certain pressures, or their viscosity increases causing the pressure medium to behave like a solid within the timescale of the experiment. The amount of 'nonhydrostaticity' is given by the ratio of the compressibilities of the sample and the pressure medium as well as the volume ratio of sample and pressure medium in the sample chamber. A highly compressible sample will therefore reach the nonhydrostatic limit at much lower pressures than a less compressible sample. In the present experiments the ruby fluorescence spectrum was used to judge the pressure conditions within the DAC. The presence of a doublet was a hint of quasihydrostatic conditions over the whole pressure range used in the experiment. Furthermore, to evaluate the amount of strain, the lattice parameters were determined from Rietveld-refinement as well as single-peak fitting (figure 2), and a strain analysis by means of Williamson–Hall plots [18] was made for n-TiC and b-TiC (figure 3). The differences of the obtained values from Rietveld and single-

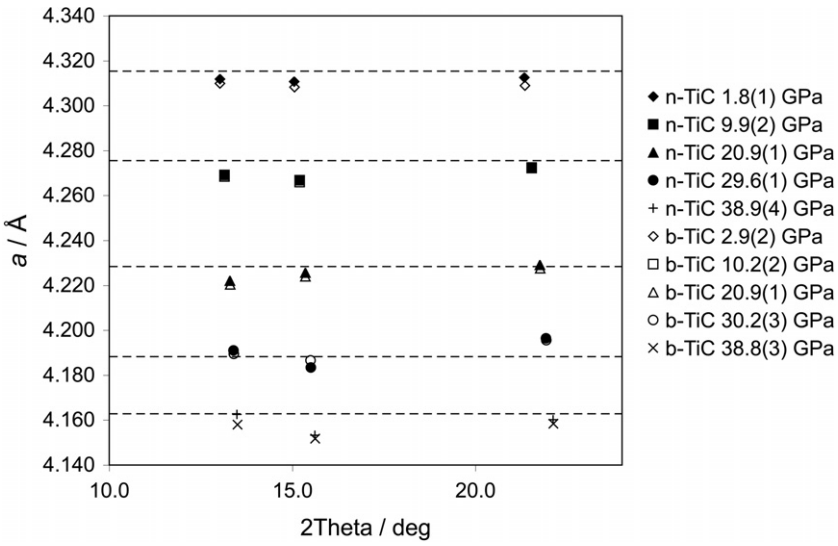

Figure 2. Lattice parameters for n-TiC and b-TiC determined from Rietveld-refinements (dashed lines) and based on single-peak fitting at comparable pressures. The errors are in the size of the symbols.

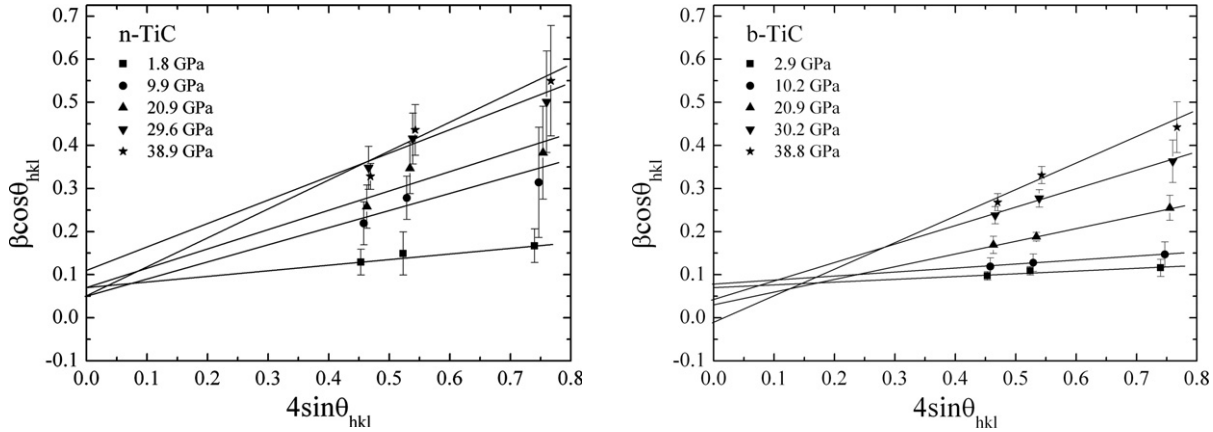

Figure 3. Williamson–Hall plots for n-TiC (left) and b-TiC (right) at different pressures. The slope of the linear fits corresponds to the amount of strain induced by the increasing nonhydrostatic conditions. The amount of strain increases with increasing pressure.

peak fitting are not significant within the experimental errors. Unfortunately, the number of observed reflections is limited to three and therefore, only qualitative statements can be given. Please note that β, the full width at half-maximum of the peak, was not corrected for the instrument broadening. From the Williamson–Hall plot, the influence of size and strain on the peak broadening can be derived. The half-width $\beta \cos \theta_{hkl}$ is plotted against $4 \sin \theta_{hkl}$, with β the full width at half-maximum of the peak and θ_{hkl} the diffraction angle. From a linear fit to the data, the strain can be extracted from the slope and the particle size from the intercept of the fit. Within the errors, the grain size for n-TiC as well as b-TiC does not change significantly as a function of pressure, in contrast to the observations for nonhydrostatic compression of gold powder [19]. Therefore, the peak broadening has to be induced by strain. This is reflected by the increasing slope of the linear fits with increasing pressure. The increase of the slope is comparable for both materials, indicating comparable conditions. The compressibility of b-TiC and n-TiC was calculated by fitting 2nd and 3rd order Birch–Murnaghan equations of state (EoS)

$$P = 3K_0 f_E (1 + 2f_E)^{\frac{5}{2}} \left[1 + \tfrac{3}{2}(K' - 4) f_E\right] \qquad (1)$$

with $f_E = [(V_0/V)^{2/3} - 1]/2$ the Eulerian strain, K_0 the bulk modulus, K' its pressure derivative, V and V_0 the unit-cell volume and volume at zero pressure, to the pressure volume data (table 1). Figure 4 shows the corresponding unit-cell volumes as a function of pressure fitted by using a 3rd order Birch–Murnaghan EoS. There are no kinks or discontinuities observable in the curves, indicating the structural stability of both materials. Within the experimental errors, the compression behaviour of both materials is identical. Table 2 summarizes the results of this study together with the literature data for comparison. The bulk modulus of b-TiC is obtained as $K_0 = 268(2)$ GPa based on a 2nd order (fixed $K' = 4$) and $K_0 = 254(7)$ GPa, $K' = 4.8(4)$ using a 3rd order Birch–Murnaghan EoS. The values for n-TiC are comparable to these values. In figure 5, a normalized strain $F_E = P/[3f_E(1 + 2f_E)^{5/2}]$ is plotted against the Eulerian strain f_E. For $K' = 4$, a constant value and for $K' \neq 4$ a

Table 1. Unit-cell volume of n-TiC and b-TiC as a function of pressure. The volume of n-TiC was measured with increasing (P up) and decreasing (P down) pressure, b-TiC only with increasing pressure.

n-TiC (P up)		n-TiC (P down)		b-TiC	
P (GPa)	V (Å^3)	P (GPa)	V (Å^3)	P (GPa)	V (Å^3)
0.3(1)	80.75(6)	0.3(1)	80.38(6)	0.7(1)	80.93(6)
1.8(1)	80.36(6)	6.4(3)	78.68(6)	1.8(1)	80.45(6)
3.1(2)	79.91(6)	15.1(3)	76.63(6)	2.9(2)	80.18(6)
5.4(1)	79.17(6)	17.9(5)	75.91(6)	4.6(2)	79.75(6)
6.6(1)	78.96(6)	21.6(6)	75.37(5)	5.8(1)	79.4(6)
8.5(2)	78.52(6)	24.6(5)	74.82(6)	6.7(2)	79.11(6)
9.9(2)	78.16(6)	29.0(7)	74.08(6)	8.2(2)	78.65(6)
12.2(3)	77.52(6)	31.8(7)	73.52(5)	10.2(2)	78.17(6)
14.5(1)	77.11(5)	33.7(6)	73.20(5)	11.9(2)	77.71(6)
15.8(2)	76.69(5)			13.5(1)	77.34(5)
18.3(1)	76.10(5)			15.0(1)	77.02(5)
20.9(1)	75.60(5)			17.7(1)	76.41(5)
22.4(1)	75.16(5)			18.7(1)	76.12(5)
22.5(1)	75.41(5)			20.1(2)	75.67(5)
25.9(3)	74.56(5)			20.9(1)	75.66(5)
28.8(2)	74.07(5)			22.0(2)	75.31(5)
29.6(1)	73.47(5)			23.4(2)	75.03(5)
30.1(1)	73.48(5)			26.2(2)	74.61(5)
34.0(4)	73.00(5)			30.2(3)	73.89(5)
38.9(4)	72.14(5)			34.1(3)	73.06(5)
				38.8(3)	72.17(5)

Table 2. Compressibility of bulk and nanocrystalline TiC. BM2 denotes a second order, BM3 a third order Birch–Murnaghan equation of state.

Material	EoS	K_0 (GPa)	K'	Reference
b-TiC	BM2	268(2)	4	This work
b-TiC	BM3	254(7)	4.8(4)	This work
b-TiC	BM3	235(2)	6.5	[9]
n-TiC	BM2	268(4)	4	This work
n-TiC	BM3	276(14)	3.5(8)	This work

linear dependency of F_E from f_E should be obtained [15]. Within the experimental errors, both curves do not differ much from a constant value, indicating good agreement of the 2nd and 3rd order fits of the Birch–Murnaghan EoS. The value of the bulk modulus reported by [9] is smaller than our values. Combined with the higher value of $K' = 6.5$ compared to $K' < 5$ from our measurements, this can be expected. The difference of the values could be due to the nonhydrostatic pressure conditions used in their experiment (see next paragraph). It also has to be noted that we did not observe a critical pressure for an irreversible stiffening as reported for Si_3N_4 and Ge_3N_4 [20, 21]. These authors found an irreversible stiffening of the nanoparticles up to a critical pressure above which the stiffness revealed the value of the microcrystalline material. A possible explanation to this discrepancy could be that their material was produced by a shock-wave synthesis, the TiC nanoparticles we used by a gas phase process. Therefore, it could be expected that the particles Dubrovinskaia *et al* [9] studied have a much higher amount of internal strain compared to the n-TiC used in this study.

Nonhydrostatic conditions. To generate nonhydrostatic pressure conditions, no pressure medium was used and the pressure chamber densely filled with the sample material. In this case, a peak splitting is observed at pressures above 20 GPa and affects all observed reflections except 200. Figure 6 shows the obtained profiles of the 111 reflection of n-TiC, b-TiC and b-TiC without pressure medium at comparable pressures. The splitting can be attributed to two phases, i.e. the cubic phase and a rhombohedrally distorted phase [9] and disappears after pressure release. The reported phase transition may therefore be induced by the nonhydrostatic conditions. Dubrovinskaia *et al* [9] used CsI as a pressure medium, which is probably not soft enough to ensure quasihydrostatic conditions as were claimed in their paper. Recently, Giefers *et al* [22] reported on a comparable observation for PbO, for which a shear-induced phase transition was only observed in the experiments using

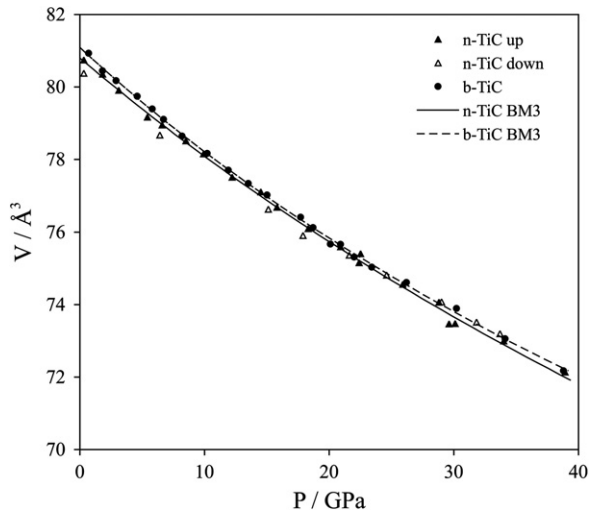

Figure 4. Unit-cell volume as a function of pressure for n-TiC and b-TiC. The solid and dashed lines represent best fits of 3rd order Birch–Murnaghan equations of state. The errors in pressure and volume are in the size of the symbols.

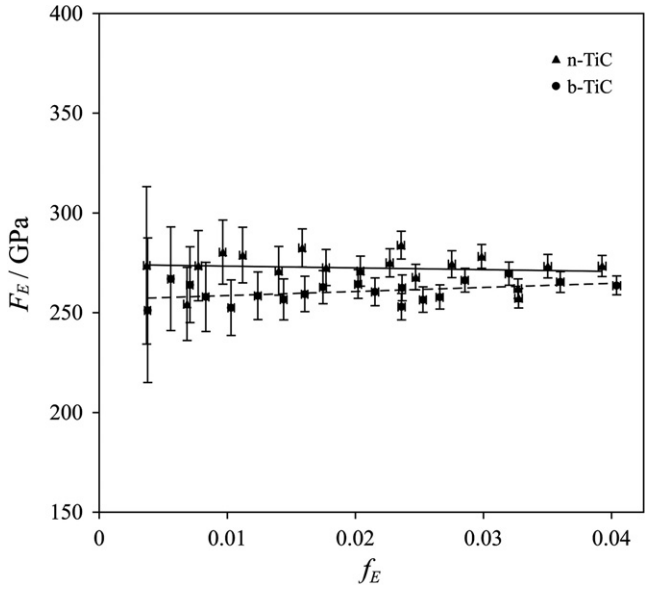

Figure 5. f_E–F_E plot for n-TiC and b-TiC. The solid and dashed lines represent the lines of best fit for n-TiC and b-TiC, respectively. The errors are calculated according to [15].

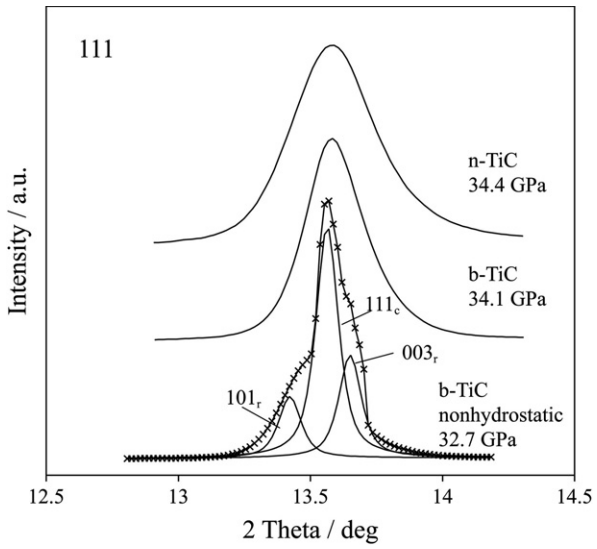

Figure 6. Profile of the 111 reflection of b-TiC and n-TiC at comparable pressures ($\lambda = 0.5640$ Å). The two upper curves are from the experiments using quasihydrostatic conditions. The lower curve illustrates the rhombohedral distortion of the structure caused by nonhydrostatic pressure conditions. The split peaks can be fitted by the 111 reflection of the cubic and the 003 and 101 reflections of the rhombohedral phase using a pseudo-Voigt profile. The indices 'c' and 'r' denote the cubic and rhombohedral phases.

a solid pressure medium. The reflection half-widths of the cubic as well as the rhombohedral phases in the nonhydrostatic environment are smaller than at quasihydrostatic conditions. A possible phenomenological explanation could be the reduction of internal strain by the structural distortion. But it has to be kept in mind that the increase of the half-widths are difficult to compare, as it is related to several experimental parameters, such as the compressibility ratios of sample and pressure medium, amount of pressure medium used, the interparticle contacts, etc [23].

3.2. Microstructure

TiC in nanoparticulate form behaves different from other nanoparticulate materials, which show an increased stiffness at smaller particle size (see e.g. [2, 3]). In general, two reasons can mainly be attributed to the difference of the nanoparticles' properties compared to those of a microcrystalline material: (i) a large surface to volume ratio; (ii) the microstructure of the nanoparticle. As is well known, a large surface to volume ratio influences many properties of the nanoparticles. An upper limit for a significant influence on physical properties is commonly accepted to be a particle size of less than 10–20 nm. The presently used n-TiC has a larger particle size of 30–50 nm, therefore a strong influence of the surface to volume ratio can be ruled out. Also for larger particles, the influence of the microstructure cannot be neglected. Recent studies have indicated a significant contribution of the microstructure to the change of the physical properties of the nanoparticles [3, 8]. Based on the comparable values of the compressibilities of b-TiC and n-TiC, it could be expected that the nanoparticles will have microstructures close to single crystals or at least

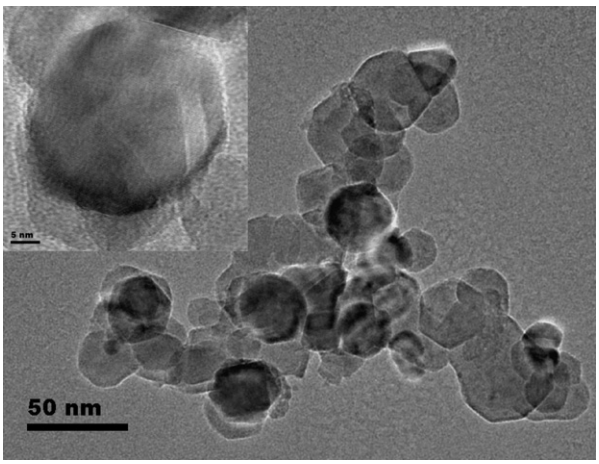

Figure 7. TEM image of the investigated n-TiC particles indicating their size distribution (30–50 nm). The inset shows an HRTEM image of a typical particle.

consist of large single-crystalline domains, as they are too big for size-induced effects. To characterize the microstructure of the nanoparticles, we performed HRTEM investigations. Figure 7 shows images of some typical particles, illustrating the size distribution and the microstructure of the particles used in this study. As was expected, nearly no twin- or grain-boundaries can be observed within the particles. The undisturbed microstructure in combination with the particle size explain well the comparable properties of b-TiC and n-TiC.

4. Conclusion

Microcrystalline and nanoparticulate TiC show a comparable compressibility. This can be understood based on the particle size and the microstructure of the investigated nanoparticles. The result may provide reasonable clues to the understanding of the contradictory compressibility behaviours of nanoparticles reported in literature. A formerly reported phase transition in b-TiC could possibly be induced by the chosen experimental conditions. Within our studies under nonhydrostatic conditions, the cubic structure of b-TiC is reversibly rhombohedral distorted above ca 18 GPa. This transition was not observed under quasihydrostatic conditions.

Acknowledgments

Part of this work was performed at the Swiss Light Source, Paul Scherrer Institut, Villigen, Switzerland. Experimental assistance from the staff of the MS beamline is gratefully acknowledged. We thank Mr H Hürlimann, University of Basel, for kindly performing the carbon analysis. This work was financially supported by the Swiss National Science Foundation under grant no. 200021-115871.

References

[1] Rekhi S, Saxena S K, Ahuja R, Johansson B and Hu J 2001 *J. Mater. Sci.* **36** 4719
[2] Jiang J Z, Olsen J S, Gerward L and Morup S 1998 *Europhys. Lett.* **44** 620

[3] Gu Q F, Krauss G, Gramm F, Cervellino A and Steurer W 2008 *Phys. Rev. Lett.* **100** 045502
[4] Gilbert B, Zhang H, Chen B, Kunz M, Huang F and Banfield J F 2006 *Phys. Rev.* B **74** 115405
[5] Tolbert S H and Alivisatos A P 1995 *Annu. Rev. Phys. Chem.* **46** 595
[6] Wang Z, Daemen L L, Zhao Y, Zha C S, Downs R T, Wang X, Wang Z L and Hemley R J 2005 *Nat. Mater.* **4** 922
[7] Wang H, Liu J F, Wu H P, He Y, Chen W, Zeng Y W, Wang Y W, Luo C J, Liu J, Hu T D, Stahl K and Ziang J Z 2006 *J. Phys.: Condens. Matter* **18** 10817
[8] Gilbert B, Huang F, Zhang H, Waychunas G A and Banfield J F 2004 *Science* **305** 651
[9] Dubrovinskaia N A, Dubrovinsky L S, Saxena S K, Ahuja R and Johansson B 1999 *J. Alloys Compounds* **289** 24
[10] Jones A P 2007 *Eur. J. Mineral.* **19** 771
[11] Hammersley A P, Svensson S O, Hanfland M, Fitch A N and Häussermann D 1996 *High Press. Res.* **14** 235
[12] Larson A C and Von Dreele R B 2000 General Structure Analysis System (GSAS) *Los Alamos National Laboratory Report* laur 86-748 edn
[13] Toby B H 2001 *J. Appl. Crystallogr.* **34** 210
[14] Miletich R, Allan D R and Kuhs W F 2000 *Rev. Mineral. Geochem.* **41** 445
[15] Angel R J 2000 *Rev. Mineral. Geochem.* **41** 35
[16] Toby B H 2005 *J. Appl. Cryst.* **38** 1040
[17] Christensen A N 1978 *Acta Chem. Scand.* A **32** 89
[18] Williamson G K and Hall W H 1953 *Acta Metall.* **1** 22
[19] Singh A K, Liermann H P, Saxena S K, Mao H K and Usha Devi S 2006 *J. Phys.: Condens. Matter* **18** S969
[20] Wang Z, Zhao Y, Schiferl D, Qian J, Downs R T, Mao H-K and Sekine T 2003 *J. Phys. Chem.* B **107** 14151
[21] Wang Z, Zhao Y, Schiferl D, Zha C S, Downs R T and Sekine T 2003 *Appl. Phys. Lett.* **83** 3174
[22] Giefers H and Porsch F 2007 *Physica* B **400** 53
[23] Singh A K 2004 *J. Phys. Chem. Solids* **65** 1589